



## Analysis of Continuous Fields

The paradigm of continuous fields provides a rich foundation for spatial modelling, particularly when data are held in regular square rasters (grids). Methods of map algebra allow mathematical operations to be carried out on whole raster overlays just as easily as if each overlay were only a single number and thus facilitates the writing of numerical models. Mathematical operations on continuous fields can be divided into point operations and spatial operations. Point operations are the same as those discussed for attributes in Chapter 7; spatial operations include spatial filtering, the computation of surface derivatives (slope, aspect, convexity), surface topology and drainage nets, spatial contiguity, linear and non-linear proximity determination, and properties of whole surfaces such as viewsheds, shaded relief, and irradiance calculations. In conjunction with Chapter 11, this chapter explains each of these operations; the methods are illustrated by applications in hydrology, erosion, and surface run-off.

- ▶ have developed a knowledge of some key ways of analysing data on continuous fields
- ▶ be able to apply your knowledge to analyse grids in combination, using map algebra, and separately, using spatial filters and other grid operators
- ▶ be able to assess surface form using slope (gradient), aspect, and other derivatives.

As we explained in Chapter 2, there are two main ways of representing continuous fields. The first is the Delaunay triangulation (the TIN of digital elevation modelling); the second is the more common altitude matrix or grid used in raster GIS and image analysis. Delaunay networks are often used outside GIS to support the finite element modelling of dynamic flow processes in groundwater movement (MODFLOW—Harbaugh 2005), discharge over floodplains (see Di Baldassare 2012 for an extensive review), or air quality (Oliver et al. 2012).

Canelli et al. (2012) discuss construction of surfaces for transport and dispersion modelling in GIS contexts. Finite element modelling (FEM) is not usually part of the standard generic toolkit of most GIS. Numerical models that use FEM are usually loosely coupled to the GIS, with the GIS being used to assemble the data and pass them to the model via an interface. The results from the model

### Learning objectives

By the end of this chapter, you will:

- ▶ understand some key concepts and classes of approaches which can be used to work with continuous fields



that the grid has already been created. Remember that the range of the variogram can be used to define the radius of the interpolation search radius (Chapter 9).

Interpolation is often a complicated operation, and while interpolation operations can be expressed in a mathematical command language many users will encounter specialist packages so that standard terminology cannot be used.

### 10.3 Spatial analysis using square windows

#### Spatial filtering

The simplest and perhaps most widely used method of spatial filtering is a discrete, continuous surface involves passing a square window (otherwise known as a kernel or filter) over the surface and computing a new value of the central cell of the window  $C_{ij}$  as a function of the cell values covered by the window. This kind of operation is also commonly known as convolution. The window is frequently of size  $3 \times 3$  cells, but any other kind of square window ( $5 \times 5$ ,  $7 \times 7$  cells, or distance measurements) is possible. The general equation is:

$$C_{ij} = f \left( \sum_{i-m}^{i+m} \sum_{j-n}^{j+n} c_{i,j} \lambda_{i,j} \right)$$

where  $f$  stands for a given window operator on windows of sides  $2m+1$ ,  $2n+1$ , and  $\lambda_{i,j}$  is a weighting factor.

$c_{i-1,j-1}$	$c_{i,j-1}$	$c_{i+1,j-1}$
$c_{i-1,j}$	$c_{i,j}$	$c_{i+1,j}$
$c_{i-1,j+1}$	$c_{i,j+1}$	$c_{i+1,j+1}$

to the central cell by introducing weights that are non-linear—i.e. those cells closest to the central cell have larger weights than those further away, much like the idea of distance weighting in ordinary interpolation.

For example, for a  $3 \times 3$  window:

1	1/15	2/15	1/15
2	2/15	3/15	2/15
3	1/15	2/15	1/15

or for a  $5 \times 5$  window:

1	1/65	2/65	3/65	2/65	1/65
2	2/65	3/65	4/65	3/65	2/65
3	3/65	4/65	5/65	4/65	3/65
4	2/65	3/65	4/65	3/65	2/65
5	1/65	2/65	3/65	2/65	1/65

RANGE →

DIVERSITY →

TOTAL →

MIN →

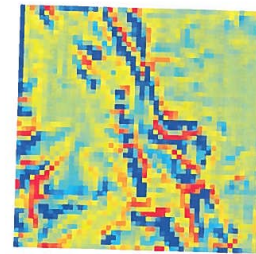
MAX →

STD DEV →

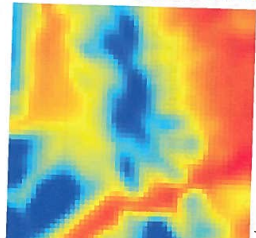
MEAN →

MODE →

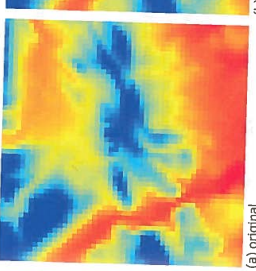
Figure 10.3 Window operations for spatial filtering



(a) original



(b) low-pass 3 x 3 filter



(c) high-pass = original - low-pass

Figure 10.4 Smoothing a surface with a low-pass filter

The low-pass filter has the effect of removing extremes from the data, producing a smoother image (Figures 10.4 and 10.5). For nominal and ordinal data (and also integer and ratio data) the mean can be replaced by the mode, which is the most common value (majority). Using a modal filter on nominal data (e.g. soil units) can be a useful way of simplifying a complex map (Figure 10.6), but note that smoothing a gridded image with a modal filter is a different kind of operation than the procedure of generalizing a map by reclassifying the attributes and merging the soil polygons given in Chapter 7.

#### Generic commands for filtering

##### To compute low-pass and high-pass filters:

**Low-pass = windowaverage (continuous\_surface, n)**

**High-pass = continuous\_surface - low-pass**  
where  $n$  is the side of the square window in cells or distance units.

##### To compute a modal filter:

**Modalmap = windowmajority (continuous\_surface, n)**

The most commonly used window operations ( $f$ ) are low- and high-pass filters.

**Smoothing (low-pass) filter:** The value for the cell at the centre of the window is computed as a simple arithmetic average of the values of the other cells (Figure 10.3). In remote sensing systems and image analysis, the mean values are computed by multiplying the cell values in the window by the  $n \times m$  values in the filter. For example, for a  $3 \times 3$  filter, the mean value for the window centre can be computed by multiplying each cell value by a weight of  $1/9$  and adding all the results. For a  $5 \times 5$  window, the weight of each cell is  $1/25$ . Extra weights can be given

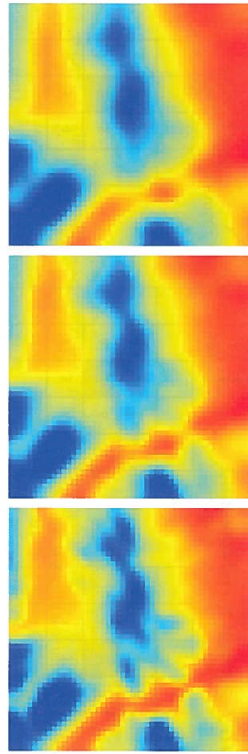


Figure 10.5 The effect of increasing window size on smoothing

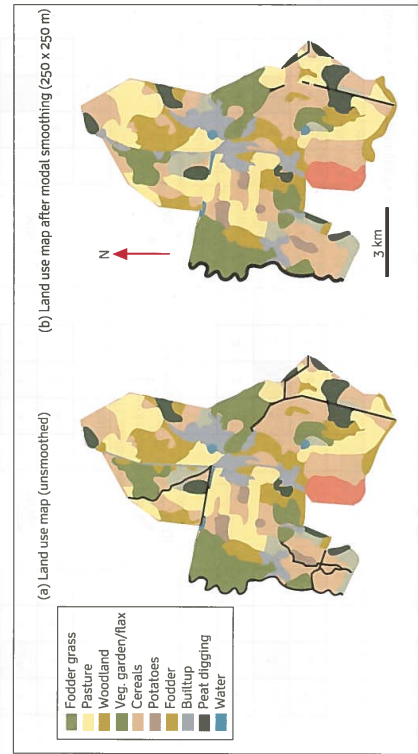


Figure 10.6 Smoothing a complex polygon map with median smoothing aggregates areas but does not reduce the number of classes (cf. Figure 7.4)

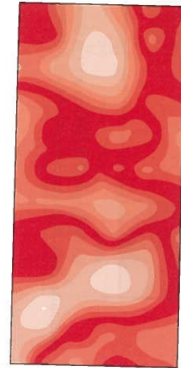
In a similar way, the local maximum or minimum values, and their difference—the range—can be easily computed. **Diversity** (the number of different values in the window) or the differences between two cells on any one of the four directional axes within the window are alternative options. For nominal and ordinal data, the minority (the least common) and the diversity are useful operations for indicating the local complexity of the spatial pattern.

**High-pass and edge filters** The inverse of the low-pass filter is one that enhances the short-range spatial properties of the continuous surface, enhancing areas of rapid change or complexity. The high-pass filter is defined as:

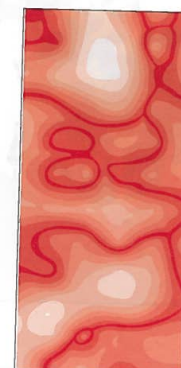
$$\text{Original surface} - \text{low-pass image} = \text{high-pass image}$$

10.5

(a) Original surface



(b) High-pass filter



(c) Maximum rate of change yields boundaries

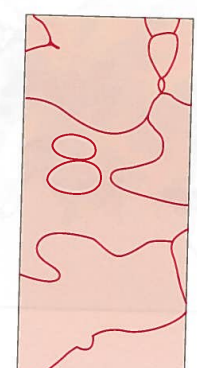


Figure 10.7 Using an edge filter to extract boundaries

#### 10.4 Filtering case studies

207

The qualities of the high-pass filter can therefore depend on how the low-pass filter is defined. Alternatively, a set of weights can be defined for the window (Pavlidis 1982). A commonly used set of weights is the Laplacian filter:

0	1	0
1	-4	1
0	1	0

Figure 10.7 shows an example of applying an edge filter to determine the locations of maximum rates of change in a continuous surface. Edge filters are also used to enhance relatively uniform areas in the continuum provided by a remotely sensed image. The derivation of sharp edges and sets of boundary pixels is often used for inferring the presence of discrete spatial entities in the image, which ultimately could be extracted and vectorized as required.

#### 10.4 Filtering case studies

This section builds on the discussion above by introducing two case studies which are intended to show how filters can be used to modify the characteristics of raster data. Case study 10.1 deals with a continuous property—specifically, elevation in Wales. Case study 10.2 demonstrates filtering of an orthoimage of part of Washington, D.C. These examples illustrate how filters can be used to smooth images (mean and median filters) or enhance contrast in some way (by generating the high-pass image or by applying a local measure of variability, such as the standard deviation).

##### Case study 10.1 Filtering elevation data for Wales

Figure 10.8 shows a DEM of Wales, with a spatial resolution of 661 m. In Figure 10.9, the output of a  $3 \times 3$  mean filter is shown. The range of data values is clearly smaller than in the original image although, as with the mean filter output, the general pattern of elevation values is the same. The original grid (Figure 10.8)—so Figure 10.9 presents a smoothed version of the original DEM.

Figure 10.10 is given in Figure 10.9. This is termed a high-pass image, as defined

**Case study 10.1 (continued)**

in equation 10.5, and notable breaks of slope are particularly clear in this map. Figure 10.12 shows the output of the standard deviation filter, which highlights areas of local contrast in elevation values.

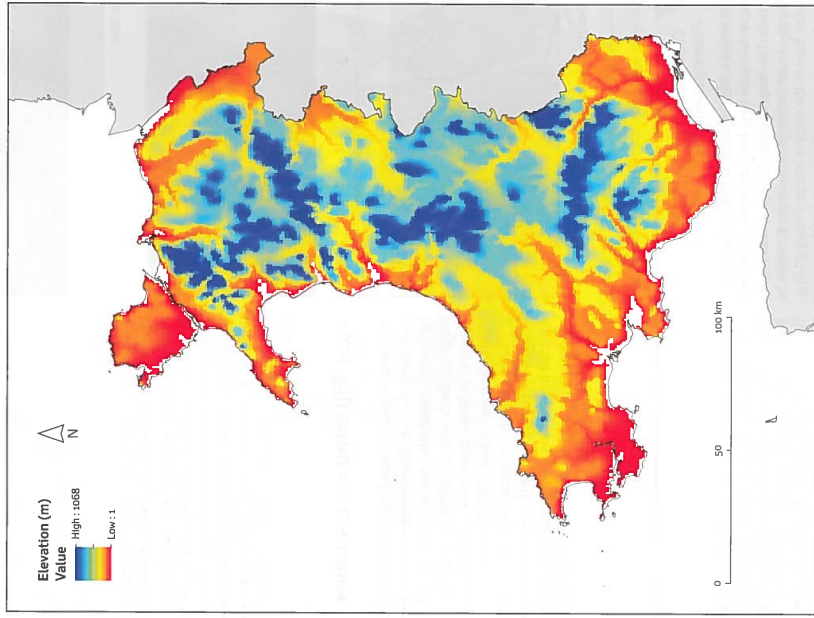


Figure 10.8 Digital elevation model of Wales; spatial resolution of 664 m (image courtesy of the US Geological Survey)

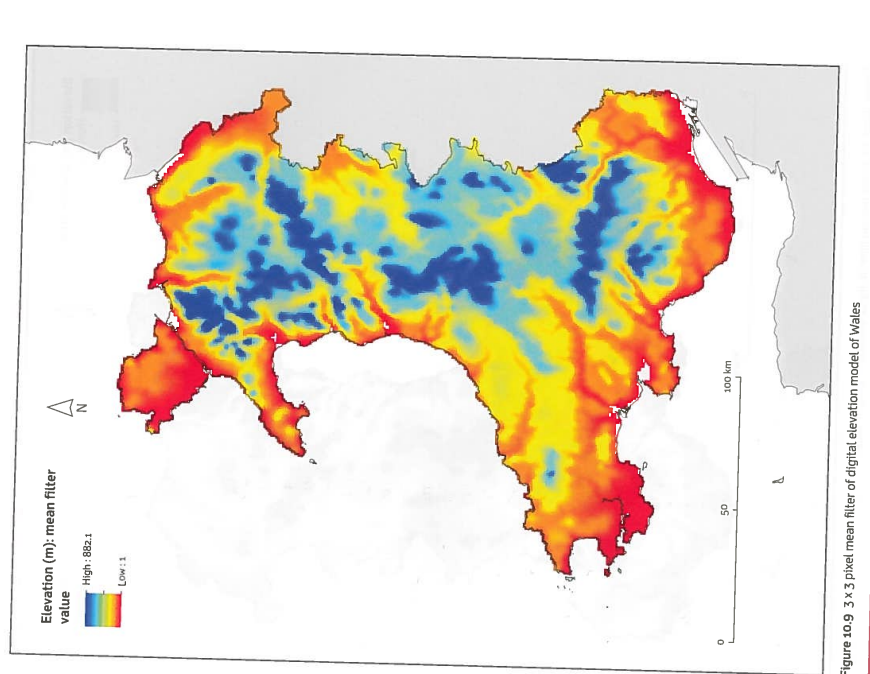
**Case study 10.1 (continued)**

Figure 10.9 3 x 3 pixel mean filter of digital elevation model of Wales

## Case study 10.1 (continued)

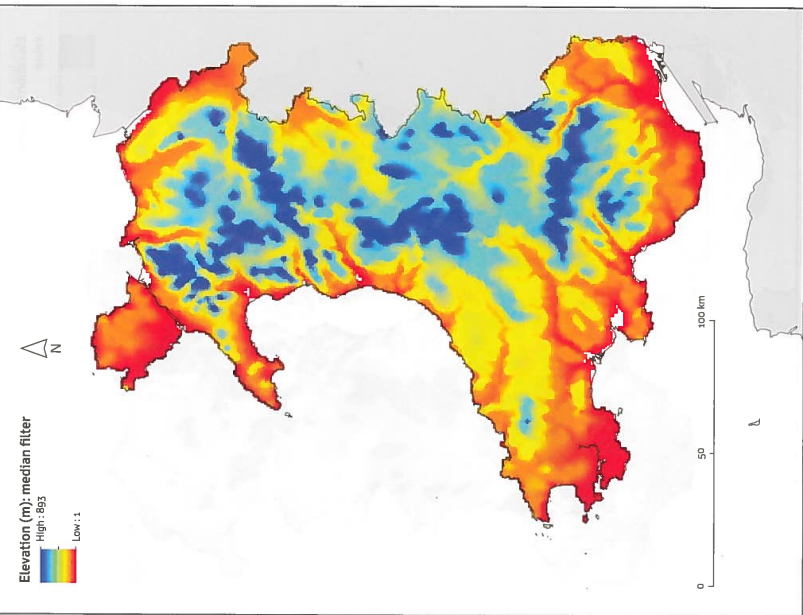


Figure 10.10 3 × 3 pixel median filter of digital elevation model of Wales

## Case study 10.1 (continued)

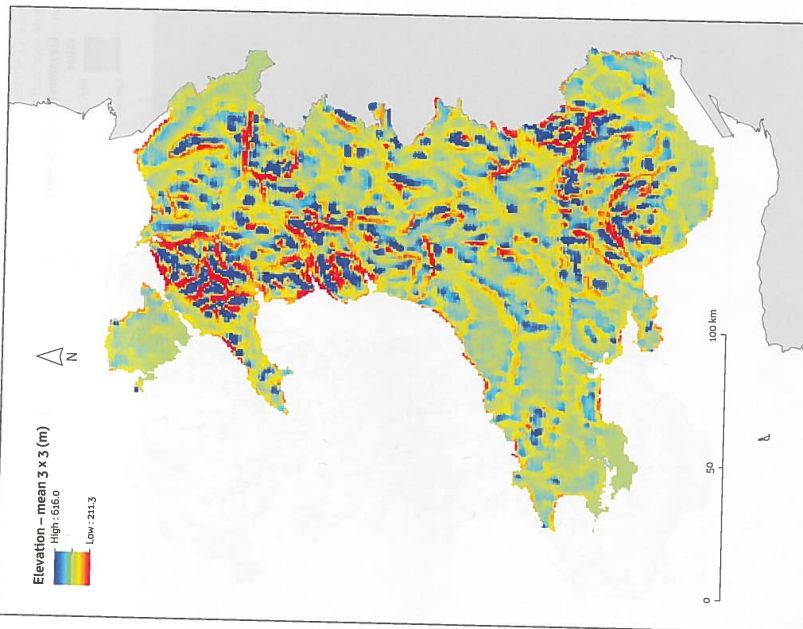


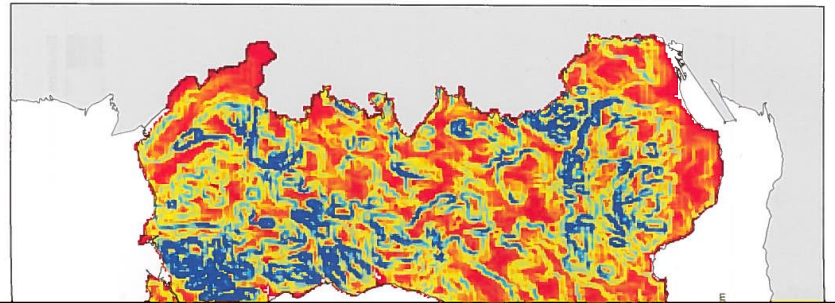
Figure 10.11 Elevation minus 3 × 3 mean filter

**Case study 10.2**  
**Enhancing contrast with filters in Washington, DC**

A set of filters were also applied to an orthomosaic (geometrically corrected aerial image) of a part of Washington, DC. The image is shown in Figure 10.13. Moving windows of 3x3 (Figure 10.14), 21 x 21 (Figure 10.15) and 51 x 51 (Figure 10.16) pixels were applied for deriving the local means. Note that the White House has been blocked out' by the data suppliers as a security measure, and thus appears uniform. Figure 10.17 gives the 3 x 3 pixel standard deviation. The White House buildings show clearly, as do the street network and other buildings in this part of the city.



Figure 10.13 Orthomosaic of part of Washington, DC; spatial resolution: 0.3 m (image courtesy of the US Geological Survey)



**Case study 10.2 (continued)**

Figure 10.14 3 x 3 pixel mean filter of orthoimage of part of Washington, DC

**Case study 10.2 (continued)**

Figure 10.15 21 x 21 pixel mean filter of orthoimage of part of Washington, DC

## Case study 10.2 (continued)

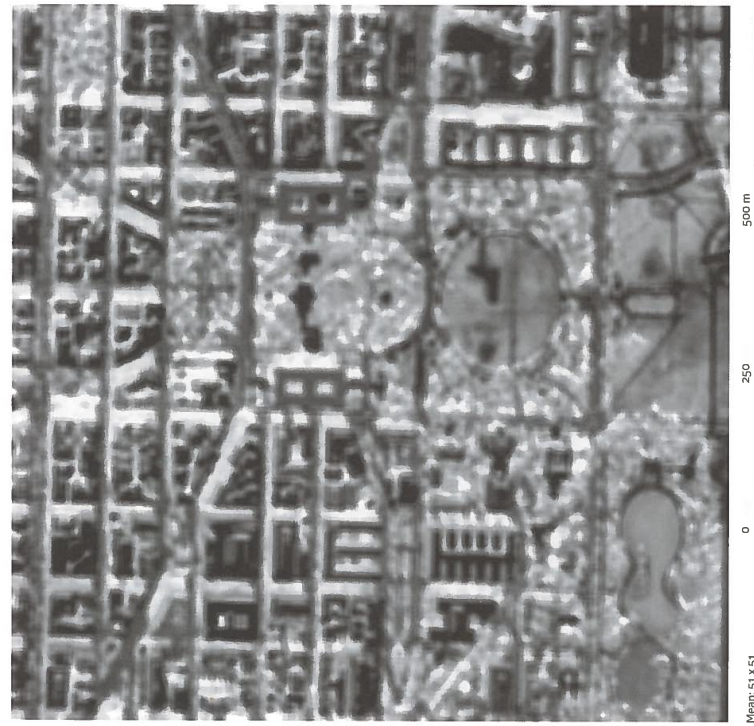


Figure 10.16 5x5 x 51 pixel mean filter of orthoimage of part of Washington, DC

## Case study 10.2 (continued)

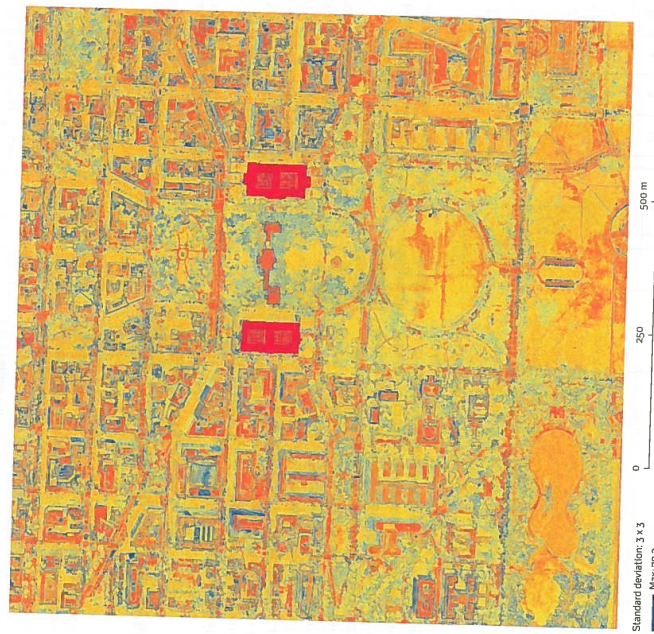


Figure 10.17 3x3 pixel standard deviation filter of orthoimage of part of Washington, DC

## 10.5 Other grid operators

The chapter has so far focused primarily on focal operators such as the smoothing filter. This section describes some other key classes of grid operators.

This section describes some other key classes of grid operators. Measurement of cell distances from prespecified source cells is a common objective—Figure 10.18 shows distances of all cells in a grid from two source cells (the shaded cells). In this case, the distances are in cell units and refer to distance from the nearest source cell to each cell in the grid. It is easy to think of potential applications for this approach given that distances are central to many spatial analysis operations. Chapter 7 dealt with, among other topics, overlay between discrete features. Similarly, with raster data, it is sometimes necessary to ascertain which data values fall within particular zones or areas and to summarize these data values in some way. Operators which allow for this kind of analysis are known as **zonal operators**.

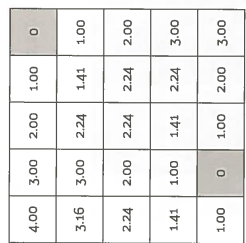


Figure 10.18 Euclidean distances from source cells (shaded)—the shortest distance from either of the two source cells is given

value is divided by the number of cells in the zone, giving  $33/7 = 4.7$ . So given a set of zones (note that cells in zones do not need to be contiguous), the overlapping data values can be summarized using any standard statistical summary including the minimum, maximum, mean, and sum. Sonwalkar et al. (2010) apply the zonal function to summarize NDVI (Normalized Difference Vegetation Index) values in particular soil types.

## 10.6 Other cell-based analysis operations

The cell-based operations for continuous fields given here are merely the most common subset found in GIS and image analysis. Other operations of similar type have been developed in the areas of mathematical morphology (see Shih 2009) and cellular automata (see Liu 2008). **Temporal change** With gridded data it is very easy to adapt the operations given in this chapter and also the attribute calculations of Chapter 7 in such a way that they can be carried out many times, thereby providing a means to model dynamic processes. Most operations with cellular automata involve temporal change.

Figure 10.19 gives an example of zonal sum and zonal mean. In words, the cell values (top left) which overlap with each zone (top right) are identified and summarized. For example, in the case of the zonal sum, the values which fall within zone 3 are summed:  $5 + 3 + 7 + 5 + 4 + 6 = 33$ . The value 33 is then written to all of the zone 1 cell locations in the output—so the value 33 appears in the output in each of the seven cells which correspond to zone 1. For the zonal mean, the summed

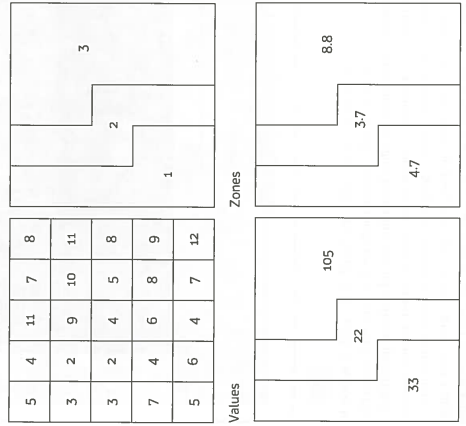


Figure 10.19 Zonal sum and zonal mean operators, given the values in the top-left and the zones on the top-right, and the resulting zonal sum and zonal mean.

## 10.7 First and higher order derivatives of a continuous surface

Chapter 11 focuses on one form of continuous surface—the digital elevation model (DEM). The remainder of this chapter introduces some key products which can be derived from DEMs, providing some context for Chapter 11. For the purposes of this chapter, a DEM is defined as a model of a physical surface—in the case of a raster-based model, the cells of the grid are elevations about some arbitrary datum. Detailed discussions about DEM types and sources, as well as further methods for their analysis, are provided in Chapter 11.

Because the gridded surface is supposed to be mathematically continuous, it is in principle possible to calculate the mathematical derivatives at any location. In practice, because the surface has been discretized, the derivatives are approximated either by computing differences within a square filter or by fitting a polynomial to the data within the filter. The two first order derivatives are the slope and the aspect of the surface; the two second order derivatives are the profile convexity and plan convexity (Evans 1980). Slope is defined by a plane tangent to the surface as modelled by the DEM at any given point, and comprises two components: gradient (the maximum rate of change of altitude) and aspect (the compass direction of this maximum rate of change). These terms follow the terminology of Evans (1980); many users of GIS packages use 'slope' to mean 'gradient' as just defined. Gradient and aspect are sufficient for many purposes, being the first two derivatives of the altitude surface or hypsometric curve, but for geomorphological analysis, the second differentials, convexity (the rate of change of slope expressed as plan convexity and profile convexity) and concavity (i.e. negative convexity), are also useful. Gradient is usually measured in per cent, degrees, or radians, aspect in degrees (converted to a compass bearing), while convexity is measured in degrees per unit of distance (e.g. degrees per 100 m).

### Using directional filters to estimate slope and aspect

The derivatives of the hypsometric curve are usually computed locally for each cell on the altitude matrix from data within a  $3 \times 3$  cell kernel or 'window' that is successively moved over the map (Figure 10.20). The simplest finite difference estimate of gradient in the  $x$  direction at point  $i,j$  is the *maximum downward gradient*:

$$[\delta z / \delta x]_{ij} = \max[(z_{i+j} - z_{i-j}) / 2] / dx$$

where  $\delta x$  is the distance between cell centres. (Note that for comparisons along diagonals the  $\sqrt{2}$  correction to  $\delta x$  should be applied to reflect the greater distance between cell centres; see Section 10.8.) This estimator has the disadvantage that local errors in terrain elevation contribute quite heavily to errors in slope. A better, much-used second-order finite difference method (Zevenbergen and Thorne 1987) uses a second order finite difference algorithm fitted to the four closest neighbours in the window. This gives the slope by

$$\tan A = [(\delta z / \delta x)^2 + (\delta z / \delta y)^2]^{1/2}$$

where  $z$  is altitude and  $x$  and  $y$  are the coordinate axes.

The aspect is given by

$$\tan A = (\delta z / \delta y) / (\delta z / \delta x) \quad (-p < A < p)$$

Zevenbergen and Thorne (1987) show how these attributes and the convexity and concavity are computed from a six-parameter quadratic equation fitted to the data in the kernel—see Box 10.1.

A third order finite difference estimator using all eight outer points of the window, given by Horn (1985), is:

$$[\delta z / \delta x] = [(z_{i+1,j+1} + 2z_{i+1,j} + 2z_{i+1,j-1} + z_{i+1,j-2}) - (z_{i-1,j+1} + 2z_{i-1,j} + 2z_{i-1,j-1} + z_{i-1,j-2})] / 8\delta x$$

and for the south–north gradient

$$[\delta z / \delta y] = [(z_{i+1,j+1} + 2z_{i+1,j} + z_{i+1,j-1}) - (z_{i-1,j+1} + 2z_{i-1,j} + z_{i-1,j-1})] / 8\delta y$$

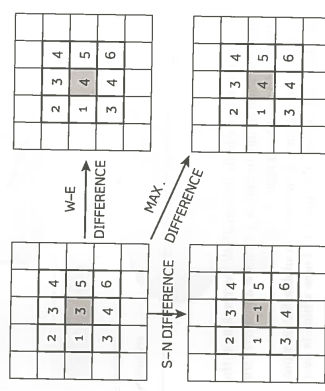
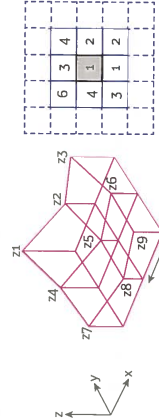
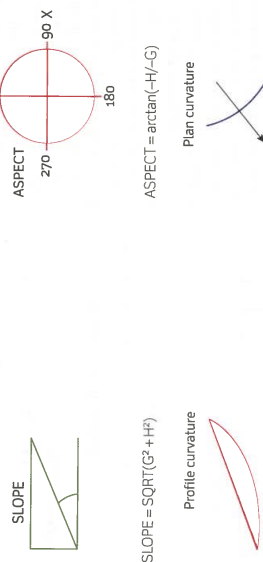


Figure 10.20 Computing derivatives with simple filters

10.6

**Box 10.1 Computing slopes using Zevenbergen and Thorne's method**

$$\begin{aligned}
 A &= [(z_1 + z_2 + z_7 + z_9)/4 - (z_2 + z_4 + z_6 + z_8)/4 + 25]/d^4 \\
 B &= [(z_1 + z_2 - z_7 - z_9)/4 - (z_2 - z_8)/2]/d^3 \\
 C &= (-z_1 + z_3 + z_7 + z_9)/4 + (z_4 - z_6)/2]/d^3 \\
 D &= [(z_4 + z_5)/2 - z_5]/d^2 \\
 E &= [(z_2 + z_8)/2 - z_5]/d^2 \\
 F &= (-z_1 + z_3 + z_7 + z_9)/4d^2 \\
 G &= (-z_4 - z_6)/2d \\
 H &= (z_2 - z_8)/2d \\
 I &= z_5
 \end{aligned}$$



$$\begin{aligned}
 \text{SLOPE} &= \text{SQRT}(G^2 + H^2) \\
 \text{Aspect} &= \arctan(-H/G) \\
 \text{Profile curvature} &= P_C = 2(DG^2 + EH^2 + FG^2 - FGH)/(G^2 + H^2)
 \end{aligned}$$

Concave = positive  
Convex = negative

**10.7 First and higher order derivatives of a continuous surface**

221

results returned by Horn's method and the polynomial method. Li et al. (2004) provide a good summary of alternative approaches. Jones (1998) has carried out another analysis of eight algorithms for computing slope and aspect using both real and synthetic DEM surfaces.

Aspect maps can be displayed by nine classes—one for each of the main compass directions N, NE, E, SE, S, SW, W, NW, and one for flat terrain (see Figure 10.22). An alternative is to use a continuous, circular greyscale which is chosen so that NE-facing surfaces are lightest; this gives a realistic impression of a 3-D surface.

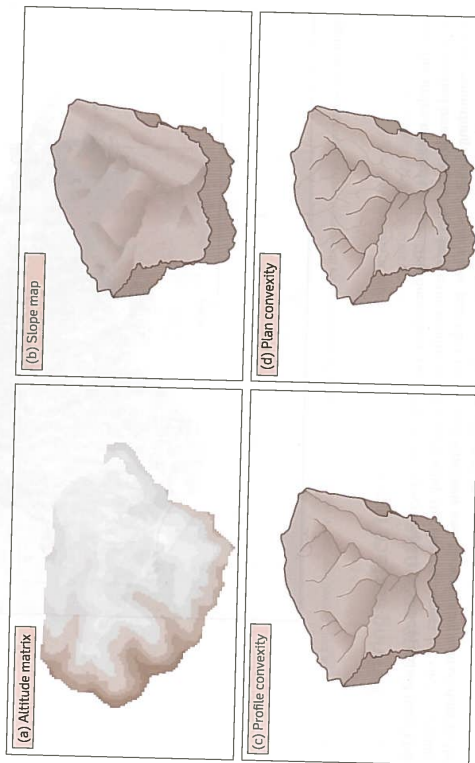
Slope often varies quite differently in different regions, and although adherents of standard classification systems usually want to apply uniform class definitions, the best maps are arguably produced by calibrating the class limits to the mean and standard deviation of the frequency distribution at hand. Six classes, with class limits at the means, the mean  $\pm 0.6$  standard deviations, and the mean  $\pm 1.2$  standard deviations usually give very satisfactory results (Evans 1980; see also Mitasova et al. 1995 for original ways of displaying slope information).

Figure 10.23 shows a map of slope using a continuous colour scale. It is a general feature of maps derived from altitude matrices that the images are more noisy than the original surface—in general, roughness increases

as the number of derivatives increases. Aspects are usually derived from the difference between the values generated by the algorithm and the true values for the test surfaces, the algorithms of Zevenbergen and Thorne (1987) and Horn (1987) perform well. These algorithms are used by several well-known GIS packages, so there is general agreement on the better algorithms. These findings are supported by Zhou and Liu (2004), whose comparison was based on deriving slope from synthetic surfaces with no data errors and with errors (random noise) added to the surfaces.

Displaying maps of slope and aspect After the appropriate derivative has been calculated for each cell in the altitude matrix, the results may need to be classified in order to display them clearly on a map. For visual ap-

preciation, display of the thematic data (slope, aspect, etc.) draped over a digital elevation model is very effective (see Section 5.6). Figure 10.21 gives examples



**Figure 10.21** First and second order derivatives of a DEM

Alternative methods fit a multiple regression to the nine elevation points in the  $3 \times 3$  window and derive the slope and aspect from that. Skidmore (1989) reviewed six methods of estimating slope and aspect, including those given in this section. He concluded that both the second and third methods given above were superior to the simple algorithm in equation 10.6, but that there was little difference in the

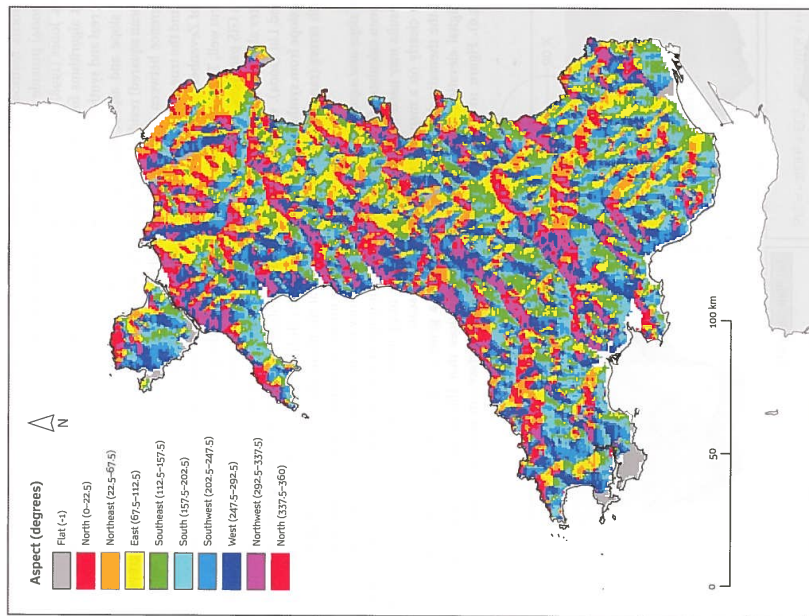


Figure 10.22 Aspect map, derived from digital elevation model of Wales

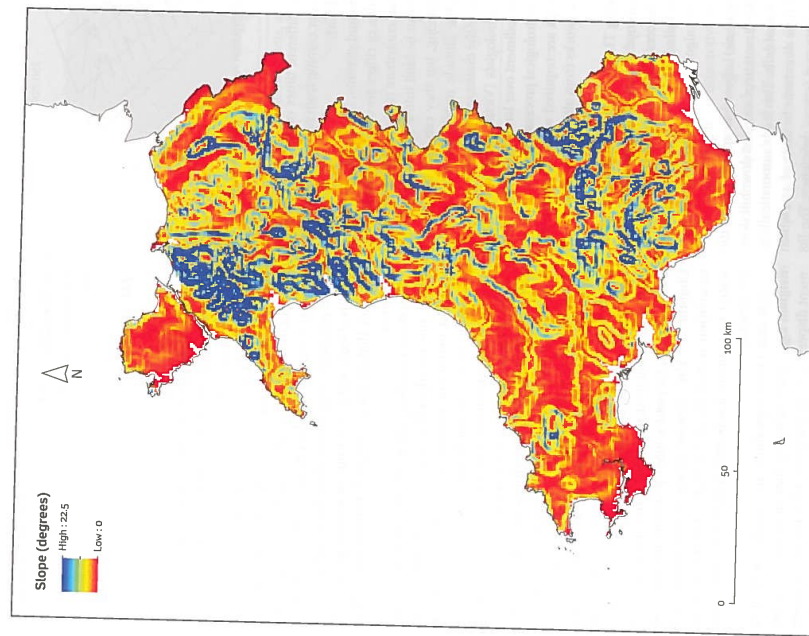


Figure 10.23 Slope map, derived from digital elevation model of Wales

with the order of the derivative. The derivatives can be smoothed by a low-pass filter before the results are plotted. Smoothing the DEM with a low-pass filter before computing the derivatives also reduces noise, but this is at the expense of removing the extremes from the data and results in underestimates of slope angles.

Slope and aspect maps can also be prepared from TINs by computing the slope or aspect for each triangular facet separately and then shading it according to the gradient class.

The following section defines some other key products which can be derived from DEMs.

In areas of gentle relief it is not always easy to judge by eye on aerial photographs where the boundary of a catchment should be, and under thick forest it may be difficult to even see the streams. Even on very detailed topographical maps the drainage network as represented by the drawn blue lines may seriously underestimate the actual pattern of all potential water courses. It could be useful, for example, to be able to separate water-carrying channels

## 10.8 Deriving surface topography and drainage networks

Before drainage basins and drainage networks could be analysed quantitatively, they had to be laboriously copied from aerial photographs or printed topographical maps. Besides being tedious, this work inevitably led to an increase in the

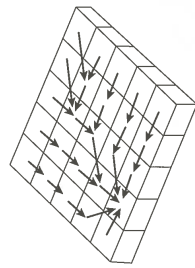


Figure 10.24 Local drain direction vectors to indicate steepest down-slope path

The resulting new grid overlay is called the set of local drain directions, or ldd (Figure 10.2a). Each cell contains a directional-type integer of value FD (flow direction) where:

FD = d \text{ where } d = \max\_{i=1,8} [w\_i - z\_{i,11}, j\_{i,11}]

The distance weight  $w_i$  is 1 for NSEW neighbours and  $1/\sqrt{2}$  for diagonals (to reflect longer distances across, rather than along, cells).

Figure 10.2b is an example of the ldd map displayed over the background of the DEM. Because of its simplicity, the D8 algorithm has been incorporated in several commercial GIS. On uniformly sloping surfaces it produces long, linear flow lines, and uniform flow directions, and it is not uncommon to get parallel flow lines that do not converge. It cannot model flow dispersion.

The Rhos (random) algorithm is a statistical version of the D8 algorithm which was introduced to represent better the stochastic aspects of terrain. It replaces the  $w_i$  of  $1/\sqrt{2}$  for diagonals by  $1/(2-r)$ , where  $r$  is a uniformly distributed random variable between 0 and 1. Moore (1996) claims that this simulates more realistic flow networks, though like the D8 algorithm it cannot model dispersion (Wilson and Gallant 2000a, 2000b). A D8-based alternative to the Rhos

which might be even more realistic can be obtained by Monte Carlo simulation. An RMS error can be added to the DEM and the D8 algorithm is used to compute a network, which is stored. This is repeated, for example 100 times, to yield a most probable network (see Chapter 12). The extra advantage of the Monte Carlo simulation is that the error on the DEM can be adjusted to realistic levels and probabilistic flow paths are generated.

**D8 and Rhos algorithms** are modifications of the original algorithms, allowing flow dispersion or catchment dispersion to be modelled. Flow can be distributed to multiple nearest-neighbour nodes in situations where there is overland flow, rather than concentration of flow in channels, where the D8/Rhos algorithms are used. The proportion of flow to the multiple downstream nodes is computed on a slope-weighted basis (Wilson and Gallant 2000b).

**Stream tube methods** Costa-Cabral and Burges (1993) determine the amount of flow as a fraction of the area of the source pixel entering each pixel downstream as determined by the intersection of a line indicating the drainage direction (aspect) and the edge of the pixel.

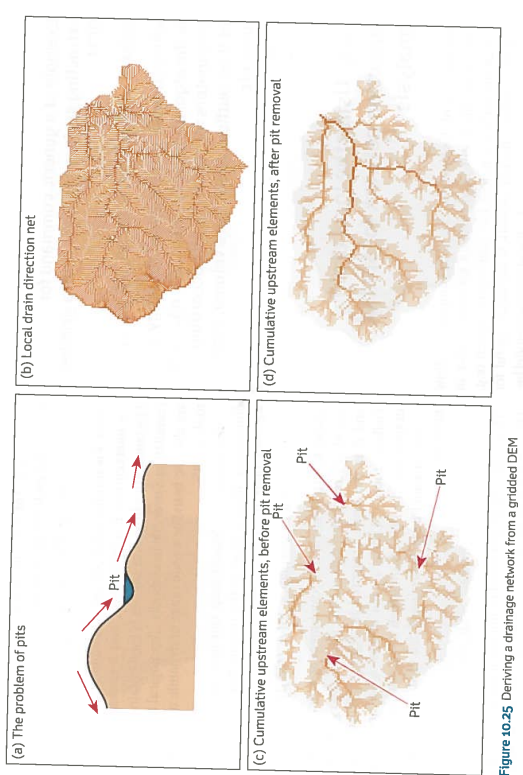


Figure 10.25 Deriving a drainage network from a gridded DEM

neighbours, and then examining whether the neighbour drains downhill to another destination. If this does not happen, the elevation is increased again until a linkage is found.

Pit removing is an interactive process regarded by some as a necessary evil. Hutchinson (1989) has developed a spline interpolator for ensuring that pits do not occur, but it is not always sensible to remove all pits automatically because closed and semi-closed depressions may be real features in some landscapes. Yamazaki et al. (2002) describe an algorithm for adjusting DEMs derived from spaceborne sensors (SRTM3 DEM; Farr et al. 2007) using drainage network information with the intention of removing pits in the DEMs.

Once pits and plateaux have been identified, then the DEM can be adjusted to remove them. For large and complex data sets with large-area pixels a practical alternative is to obtain a vector representation of the river network, convert the river vectors to grid cells, and then 'burn in' the river cells at a lower level in the drainage network.

**Example of a generic command for extracting surface topology from a gridded DEM**

`liddmap = (dem.map, a, p1, p2, p3, p4,...)`

where `liddmap` is the derived topology, `a` is the algorithm used, and `p1, p2, p3,...` are parameters for removing pits according to their outflow depth, core volume, core area, etc.

## 10.9 Using the local drain direction network for spatial analysis

ideal surface. For example, it is easy to compute a mass balance for each cell in terms of

$$S = P - I - F - E \quad 10.13$$

where  $S$  is surplus water per cell,  $P$  is input precipitation,  $I$  is interception,  $F$  is infiltration, and  $E$  is evaporation. The cumulative flow over the net is then obtained by accumulating  $S$  over the linked cells. Topological networks are also the basis for a wide range of dynamic modelling tools in GIS.

The upstream element map can itself be useful for computing other indices of the terrain. For example, a wetness index map can be defined as:

$$\text{wetnessindexmap} = \ln(A_s / \tan \beta) \quad 10.14$$

where  $A_s$  is the contributing catchment area in  $\text{m}^2$  (number of upstream elements  $\times$  the area of each grid cell) and  $\beta$  is the slope measured in degrees (Wilson and Gallant 2000). Figure 10.26a shows a wetness map draped over the DEM from which it was derived.

The Stream Power Index (see Fried et al. 2000) is defined as

$$\omega = A_s * \tan \beta \quad 10.15$$

This is directly proportional to the stream power  $P = pgf \tan \beta$ , where  $p$  is the density of water,  $g$  is the acceleration due to gravity, and  $f$  is the overland flow discharge per unit width, which is the rate of energy expenditure over time and is a measure of the erosive power of overland flow.

The Sediment Transport Index is defined as

$$\tau = [A_s / 22.13]^{0.6} [\sin \beta / 0.0896]^{1.3} \quad 10.16$$

This index characterizes the processes of erosion and deposition, in particular the effects of topography on soil loss, it resembles the length-slope factor of the Universal Soil Loss Equation (see Winchell et al. 2008) but is applicable to three-dimensional surfaces. Figure 10.26b shows that the sediment transport index can vary along the length of a stream.

### Accumulating fluxes of material over a net

Because, in a topologically correct network, each cell is linked to a downstream neighbour, it is very easy to compute attributes such as the cumulative amount of material that passes through each cell. The accumulation operator computes the new state of the cell as the sum of the original cell value plus the sum of the upstream elements draining to the cell

$$S(c_i) = S(c_i) + \sum_u^u (c_u) \quad 10.12$$

If the material value for each cell is  $1$ , the result gives the upstream element map, or in other words the cumulative number of cells upstream of the current cell that discharge through that cell. The upstream element map is usually displayed on a logarithmic scale.

If the material value is supplied from another overlay, for example effective precipitation, then the accumulation operator will compute the cumulative flow over an

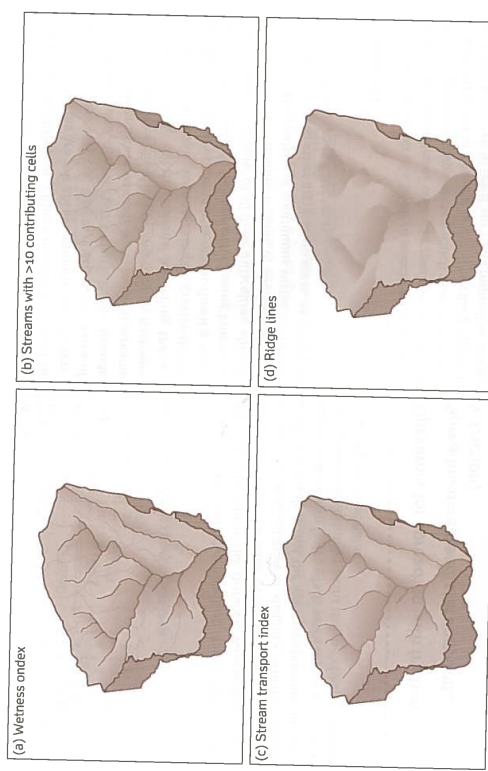


Figure 10.26 Properties derived from the drainage network

size for N-S and E-W; 1,414 for diagonals), or it can include a friction term to deal with resistances within the cells on the network (see Section 10.10).

### Difficulties with drainage nets derived from altitude matrices

Though there are many benefits of deriving the drainage network from the altitude matrix, there are also

Ridges. By definition, ridges have no upstream elements, so selecting all cells with an upstream elements value of  $0$  provides a first estimate of ridges (Figure 10.26d). Catchments. Because all cells that drain through a given cell are part of the catchment of that cell, counting upstream over the lid automatically computes the area and defines the catchment of the cell. A catchment mask can be computed by assigning a '1' to all cells in the catchment and a '0' to those outside. This can be used as a 'cookie cutter' to identify catchment-specific data from remotely sensed imagery or other sources at the same level of resolution. Using a high-pass or edge filter yields a linear catchment boundary which can be vectorized by converting the cell representation to a chain code (Chapter 3).

The stopeLength operator is similar to the accumulation operator but it computes a new attribute of a cell as the sum of the original cell value and the upstream cells, multiplied by the distance travelled over the network,  $d_u$ .

$$S(c_i) = S(c_i) + \sum_u^u (c_u d_u) \quad 10.18$$

Figure 10.27 shows slope lengths computed in this way. The distance travelled can be a simple Euclidean distance depending on the size of the cells ( $1 \times 1$  unit cell

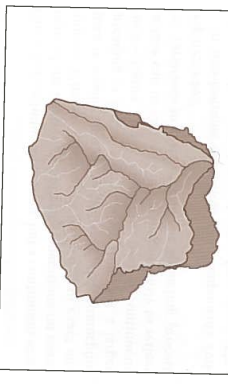


Figure 10.27 Deriving slope lengths from a DEM along the lid

several difficulties. One is the problem of modelling dispersion and diffusion. Others involve the errors in DEM—landforms are not always smooth and differentiable. The choice of cell size may affect estimates of slope, aspect, and stream connectivity. In the altitude matrix the streams are one cell wide, but real streams vary in width over their length and may be narrower or wider than the cell dimensions. Modelling the accumulation of flows assumes simple gravity-driven processes and ignores the inertia of fast-flowing water masses, which need to be approached using kinematic wave equations. In spite of all these difficulties, altitude matrix DEMs are finding a place in the hydrologist's toolkit and the analysis of continuous surfaces can lead to useful results in other application areas, as shown by the examples given in Chapter 11.

Modelling the accumulation of flows assumes simple gravity-driven

processes and ignores the inertia of fast-flowing water masses, which need to be approached using kinematic wave equations. In spite of all these difficulties, altitude matrix DEMs are finding a place in the hydrologist's toolkit and the analysis of continuous surfaces can lead to useful results in other application areas, as shown by the examples given in Chapter 11.

### Clumping

Very often the result of a Boolean selection or classification on the attributes of cells will result in sets of cells that are spatially contiguous but which cannot be identified as being part of a spatial entity. The clump operator examines every cell to see if any of its immediate neighbours in a  $3 \times 3$  window have the same class—if so, then both cells are assigned to the same clump and given a value that identifies that clump as distinct from others. The result is that each contiguous group of cells is aggregated into a larger spatial unit, which could be useful for many purposes. For example, identifying all 'ridges' via the upstream element map may create several loose aggregations of cells that belong to different ridges.

Applying the clump operator will identify each cell with a specific clump.

### 10.10 Dilatation/spreading with or without friction

This is not a window operation, but a continuous analogue of the dilation or buffering operations on exact entities. Whereas dilation (or buffering) of exact entities is usually limited to isotropic and isomorphic spreading (a buffer around a circle is just a larger circle—Figure 10.28), spreading over a continuous surface can be carried out heterogeneously to reflect the variations in resistance to the spreading process (Figure 10.29).

In non-isotropic spreading, two components contribute to the accumulation of values from the starting point. The first is distance, counted as cell steps or in

0	1	0	0	0
0	0	1	0	0
0	0	1	0	0
0	0	1	0	0
0	0	1	0	0

Figure 10.28 Isotropic spreading with grids

0	1	0	0	0
2	1	0	1	2
2	1	0	1	2
2	1	0	1	2
2	1	0	1	2

Figure 10.29 Spreading through a resistance function

real units. The second depends on the attributes of the cells through which the distance accumulation takes place. The larger the value of the 'friction' attribute, the greater the accumulation of 'distance' when traversing a cell. The result is that the effective spreading distance accumulates much faster where resistance is greatest, so that geometrically longer paths may be cheaper ways to reach a given destination.

### Operators for spreading with friction

**Spreadmap = spread((startingpoints, v, friction))**

where **startingpoints** gives the locations (cells) from which to start the spreading or buffering, **v** is an initial value, and **friction** gives the internal resistance on a cell-by-cell basis

Both simple and frictional spreading can be used to estimate slope lengths perpendicular to the stream nets derived from the upstream element maps (or from any other linear feature such as roads or railways).

### Commands to create slope length and inverse slope length

**slopeLength = spread(strm, 0, slp.map)**

**slmx = mapmaximum(slopeLength)**

**report slopeLength = ((1 - (slopeLength / slmx))\*slmx)**

where **strm** is the map of stream locations, **slp.map** is the map of slopes, and **slopeLength** is the resulting slope length perpendicular to streams

Instead of spreading over all cells, non-isotropic spreading can be confined to follow the routes defined by the lid map, or by a subset of the lid. When the resistance varies over the network this can reveal areas where flow problems might accumulate.

### \* 10.11 Summary

This chapter has demonstrated that there is a large range of products that can be derived from continuous surfaces that have been discretized as regular grids (Table 10.1). Some derived data, such as slope and aspect (and line of sight, hill shading, and irradiance, as considered in the following chapter), can also be easily obtained from TINs, but it is not usual to find systems that provide facilities for deriving the topology of the surface and for computing material flows over these derived networks. Frequently, the users of TINs will have input their networks explicitly as topologically connected lines or objects.

The most commonly encountered continuous field is the DEM, and most of the derivatives mentioned above have a direct bearing on the use and interpretation of terrain elevation. The operators presented can be used on any continuous field; however, such as remotely sensed images or the results of interpolation or spatial modelling, as will be described in the following chapter. Table 10.1 summarizes the functional capabilities of a GIS that can deal both with exact entities and continuous fields. Frequently, but not always, the continuous surfaces represent landform, as discussed in more detail in the next chapter. These methods have applications in many fields, not just including hydrology, but also erosion and land degradation studies, forest management, and soil and water pollution. Although all the examples relate to physical problems of the landscape, these kinds of analyses can also be applied to any study in which one or more attributes can be modelled as a continuous surface, such as surfaces of market potential, exposure to disease, or economic well-being.



**Table 10.1** Functional capabilities of GIS for analysis of entities and continuous fields

Geometric	Convert geographic coordinates from one projection to another
Interactive	Interactively update and edit geographic editing and attribute data
Sorting	Sort attribute or geographic data as required
Location	Locate entities having defined sets of attributes
Summarize	Summarize attributes of geographic entity (point/line/polygon/cell)
Compute statistics	Compute statistics (means, areas, enclosures, etc.) for points/lines/polylines/polys
Proximity	Conduct nearest neighbour and proximity searches—create buffer zones and carry out corridor analyses
Interpolate	Interpolate from point data to regular grid or isolines (contours)
Block diagram	Compute block diagrams of three-dimensional data
Overlay analysis	Overlay and combine several maps in either vector (polygon) or raster (grid) mode using Boolean (AND/OR/NOT) logic and arithmetical functions/operators to manipulate both the geographic and the attribute data
Polygon to raster	Convert graphic representation from polygon to grid cell representation
Edge detection	Semi-automated detection of edges of images in raster representation
Network analysis	Find shortest path along a road network with weighted route parameters for traffic density
Digital terrain analysis	Represent landform as a 3D surface Compute slope, aspect, intervisibility, rate of change of slope, shaded relief, direction of flow, determine watershed boundaries
Models	Ability to interface with simulation models

Digital Elevation Models

The shape of the surface of the earth is fundamentally important to humans. Terrain form impacts on the direction of the flow of water, the clarity of the signal received via satellite, and the amount of solar energy received.

Learning objectives

By the end of 2011

- By the end of this chapter, you will:
    - understand some key concepts and classes of approaches which can be used to work with digital elevation models
    - have developed a knowledge of some key ways of analysing digital elevation models
    - be able to apply your knowledge to analyse the relief and landscape management

The shape of the earth's surface affects a wide range of earth surface processes. DEMs are very widely used across the geosciences. DEMs are used predominantly in geomorphology, hydrology, glaciology, among other disciplines – this chapter discusses what DEMs are, and how and why they are acquired and used. A DEM may be used directly where elevation is a defining value in a study (for example, to assess the effect of flooding on a particular area or to assess the visibility of one location from another location). Alternatively, users may be interested in deriving variables from the DEM, such as

Further reading

1. Compare and contrast the effects of (a) spatial filtering and (b) polygon reclassification and entity merging, for generalizing a soil or land use map.
  2. Provide an outline of a procedure which could be used to identify edges in an image and convert the edges into vector features.
  3. Outline an application where the zonal sum operator might be useful.

Further reading

- Further Reading**

  - Li, Z., Zhu, Q., and Gold, C. (2004). *Digital Terrain Modeling: Principles and Methodology*. CRC Press, Boca Raton, FL.
  - Lloyd, C.D. (2010). *Spatial Data Analysis: An Introduction for GIS Users*. Oxford University Press, Oxford.
  - Moore, I.D. (1996). Hydrological modeling and GIS. In M.F. Goodchild, L.T. Steyaert, B.O. Parks, C.J. Johnston, D. Maidment, M. Crane, and S. Gledhill (eds), *GIS and Environmental Modeling: Progress and Research Issues*. GIS World Books, Fort Collins, CO, pp. 143–148.
  - Wilson, J.P. and Gallant, J. C. (2000). Digital terrain analysis. In J. P. Wilson and J. C.